JOURNAL OF AGRICULTURAL AND FOOD CHEMISTRY

Agricultural and Environmental Chemistry

Natural Product Neopeltolide as A Cytochrome bc1 Complex Inhibitor: Mechanism of Action and Structural Modification

Xiao Lei Zhu, Rui Z'hang, Qiong-You Wu, Yong-Jun Song, Yu-Xia Wang, Jing-Fang Yang, and Guang-Fu Yang

J. Agric. Food Chem., **Just Accepted Manuscript** • DOI: 10.1021/acs.jafc.8b06195 • Publication Date (Web): 22 Feb 2019

ACS Publications

is published by the American Chemical Society. 1155 Sixteenth Street N.W., Washington, DC 20036

Natural Product Neopeltolide as A Cytochrome bc_1 Complex Inhibitor: Mechanism of Action and Structural Modification

Xiao-Lei Zhu[†], Rui Zhang[†], Qiong-You Wu[†], Yong-Jun Song[†], Yu-Xia Wang[†], Jing-Fang Yang[†], Guang-Fu Yang[†‡]

[†]Key Laboratory of Pesticide & Chemical Biology of Ministry of Education, International Joint Research Center for Intelligent Biosensor Technology and Health of Ministry of Science and Technology, Central China Normal University, Wuhan 430079, P.R. China

[‡]Collaborative Innovation Center of Chemical Science and Engineering, Tianjin 300071, P.R. China.

Correspondence:

Guang-Fu Yang, Ph.D. & Professor

College of Chemistry

Central China Normal University

Luoyu Road 152, Wuhan 430079

P. R. China

TEL: 86-27-67867800

FAX: 86-27-67867141

E-mail: gfyang@mail.ccnu.edu.cn

Abstract:

The marine natural product neopeltolide was isolated from a deep-water sponge specimen of the family Neopeltidae. Neopeltolide has been proven to be a new type of inhibitor of the cytochrome bc_1 complex in the mitochondrial respiration chain. However, its detailed inhibition mechanism has remained unknown. In addition, neopeltolide is difficult to synthesize because of its very complex chemical structure. In the present work, the binding mode of neopeltolide was determined for the first time by integrating molecular docking, molecular dynamics simulations, and MM/PBSA calculations, which showed that neopeltolide is a Q_o-site inhibitor of the bc_1 complex. Then, according to guidance via inhibitor-protein interaction analysis, structural modification was carried out with the aim to simplify the chemical structure of neopeltolide, leading to the synthesis of a series of new neopeltolide derivatives with much simpler chemical structures. The calculated binding energies (ΔG_{cal}) of the newly synthesized analogs correlated very well ($R^2 = 0.90$) with their experimental binding-free energies (ΔG_{exp}), which confirmed that the computational protocol was reliable. Compound **45**, bearing a diphenyl-ether fragment, was successfully designed and synthesized as the most potent candidate ($IC_{50} = 12$ nM) against porcine succinate cytochrome *c* reductase (SCR). The molecular modeling results indicate that compound **45** formed a π-π interaction with Phe274 and two H-bonds with Glu271 and His161. The present work provides a new starting point for future fungicide discovery to overcome the resistance that the existing bc_1 complex inhibitors are facing.

Keywords: neopeltolide, bc_1 complex, natural product, molecular design, inhibitor

1. Introduction

Plant diseases caused by fungal pathogens have been recognized as a worldwide threat to the agricultural industry. The control of plant fungal infections is very important to the production of food and has a significant impact on human health. The bc_1 complex (also known as complex III) is one of the most important fungicidal targets.[1] The bc_1 complex is responsible for the completion of electron transfer, hydroquinone oxidation and reduction of cytochrome *c* in the mitochondrial respiratory chain. If the activity of the bc_1 complex is inhibited, the generation of ATP would be blocked, leading to cell death.[2-6] As is known, the development of strobilurin fungicides targeting the bc_1 complex (*e.g.*, azoxystrobin) has been a milestone in the fungicidal market worldwide. However, according to the Fungicide Resistance Action Committee (FRAC), an explosive increase of higher resistance has occurred worldwide for strobilurin fungicides, especially those associated with the G143A mutation in the bc_1 complex.[7-9] Therefore, an urgent demand exists to discover new fungicides to overcome the resistance to the existing strobilurin bc_1 inhibitors.

Natural products have attracted considerable attention because of their unique molecular architecture, potent biological activities, and excellent environmental compatibility.[10-11] In 2007, a new marine natural product, neopeltolide (Figure 1), obtained from a deep-water sponge specimen of the family Neopeltidae, was reported by Wright *et al*. [12] Biological assays revealed that neopeltolide could inhibit the bovine heart mitochondrial cytochrome bc_1 complex with an IC_{50} value of 2.0 nM.[13] Compared with classical inhibitors of the bc_1 complex, neopeltolide has a new chemical scaffold, making it a promising lead compound for the discovery of new fungicides to overcome the pathogen resistance that existing cytochrome bc_1 complex inhibitors are facing. However, the chemical structure of neopeltolide is too complex to be effectively synthesized, and determining how to simplify its chemical structure is a challenge. In addition, a structural-activity relationship (SAR) study showed that the carbamate-containing oxazole moiety was the key structural feature, whereas its 14-membered macrolactone moiety did not make significant contribution to its binding.[14-19] The fungicide-likeness property also needs to be improved.[20]

Until now, the inhibition mechanism of neopeltolide was unknown. Because the discovery of structurally diverse bc_1 inhibitors is of interest, herein, we studied the binding mode of

neopeltolide to the bc_1 complex *via* molecular simulations. Then, structural optimizations of neopeltolide were performed based on its binding mode. Herein, we describe the binding mechanism of neopeltolide, compare its binding mode with some other bc_1 complex inhibitors, describe process of the structural optimization of neopeltolide, and describe the inhibition effects of some newly synthesized compounds against the porcine bc_1 complex. In addition, we carried out molecular docking of these newly synthesized compounds, followed by molecular dynamics (MD) simulations and the molecular mechanics Poisson-Boltzmann surface area (MM/PBSA) calculations. Fortunately, some compounds with a simpler chemical structure were successfully obtained with significantly improved potency compared with the commercial product azoxystrobin.

2. Materials and Methods

Chemistry.

All chemical reagents and solvents purchased from commercial sources were directly used without further purification. ^{1}H NMR and ^{13}C NMR spectra were recorded on a Mercury-Plus 600 and or 400 MHz spectrometer (Varian, Palo Alto, CA) with TMS as an internal reference in DMSO-d_6 or $CDCl_3$. An Agilent 6520 Accurate-Mass Q-TOF mass spectrometer (LC/MS) (Agilent Technologies, Santa Clara, CA) was used to record high solution mass spectra. The melting points for titled compounds were determined by a B-545 melting point apparatus (Büchi, Flawil, Switzerland). Silica gel (200-300 mesh) for column chromatography was purchased from Qingdao Haiyang Chemical Co. Here, our purpose was to obtain the noted compounds quickly, but the yields of some compounds were not good.

Enzymatic Assays.

The preparation of succinate cytochrome *c* reductase (SCR, a mixture of complex II and the bc_1 complex) from porcine heart was essentially the same as reported.[23] The enzymatic activities of SCR, complex II, and the bc_1 complex were analyzed in respective reaction mixtures as reported previously. [24-26] The SCR activity was measured in a 1.8 mL reaction mixture that contained 100 mM PBS (pH 7.4), 0.3 mM EDTA, 20 mM succinate, 10 μM oxidized cytochrome

c, and an appropriate amount of SCR at 23 °C. The reaction was continuously monitored by following the absorbance change at 550 mm or 600 mm on a Perkin-Elmer Lambda 45 spectrophotometer equipped with a magnetic stirrer. The extinction coefficients used were 18.5 mM^{-1} cm^{-1} of A_{red-ox}^{550} for the cytochrome *c* reduction and 21 mM^{-1} cm^{-1} of A_{red-ox}^{600} for the DCIP reduction. To test the IC_{50} values of all compounds, the reaction was carried out in the presence of varying concentrations of the inhibitor.

Computational Methods

Molecular Docking. The three-dimensional (3D) structure of the bc_1 complex was obtained from the PDB database (PDB ID: 3CWB).[27] The AutoDock 4.2 program[28] was used to dock neopeltolide and its derivatives into the Q_o-site and or Q_i-site of the bc_1 complex. The Gasteiger charges were used for these inhibitors. To select the best set of docking parameters and to test the reliability of the docking results, the crocacin derivative (ligand in 3CWB) [27] and antimycin (the Q_i-site inhibitor) were first docked into the Q_o and Q_i sites, respectively.

In the docking process, the Solis and Wets local search method and the Lamarckian genetic algorithm (LGA) [28] were selected for the conformational search. The grid size was set to 40 × 50 × 40, and the grid space was set to 0.375 Å. The others parameters were as set as in our previous work.[23-24] Among a set of 256 candidates of docked complex structures, the best one was selected according to the interaction energy and was then compared with the conformation of crocacin derivative/antimycin extracted from the crystal structure. By tuning the docking parameters, the final inhibitor conformation in the Q_i and or Q_o sites was obtained based on the smallest root-mean-square deviation (RMSD). The RMSD between the selected conformation and that previously noted in the X-ray crystal structure was 0.79 for the Crocacin derivative and 0.85 for antimycin (data not shown), confirming the reliability of the docking parameters. The same docking parameters were used to perform molecular docking of other compounds.

Molecular Dynamics and Binding Energy Calculation. All of the complex structures derived from the molecular docking were used as starting structures for further energy minimizations using the Sander module of the Amber14 program[29] before the final binding structures were achieved. The Amber ff14 force field was used for amino acids, and the General

Amber force field was used for ligands.[30] For temperature regulation, a Langevin thermostat was used to maintain a temperature of 300 K. The bcc charges were used as the atomic charges for ligands. There were five stages for energy minimization. First, the hydrogen atom was minimized with all heavy atoms fixed. Second, all of the receptor atoms were minimized with the ligand fixed. Third, minimization was carried out with all the atoms fixed. Fourth, minimization was carried out with the backbone atoms fixed. The final minimization was performed with both the ligand and the protein relaxed. In each step, energy minimization was executed by using the steepest descent method for the first 1000 cycles and the conjugated gradient method for the subsequent 3000 cycles, with a convergence criterion of 0.1 kcal mol^{-1} $Å^{-1}$. The atomic coordinates were saved every picosecond. Then, an additional 30 ns MD simulation was performed for neopeltolide-Q_o and the neopeltolide-Q_i complex. To reduce the computational cost, only 20 ps MD simulations were performed for the newly synthesized analogs.

The binding energy of the protein-ligand complex was calculated using the MM/PBSA module.[31-32]. A detailed description of this section is provided in the Supporting Information.

3. Results and Discussion

Binding Mode of Neopeltolide. Neopeltolide was identified as a bc_1 complex inhibitor more than ten years ago; however, its detailed binding mode remained unknown. In our previous study,[24] we developed an integrated computational simulation protocol to assign Ametoctradin as a Q_o site inhibitor of the bc_1 complex for the first time, which was later experimentally confirmed by Fehr and his co-workers.[33] Herein, this computational protocol was further used to determine the detailed binding mechanism of neopeltolide.

First, the chemical structure of neopeltolide was compared with that of existing bc_1 inhibitors, such as pyribencarb and a Crocacin derivative. Interestingly, the key carbamate moiety of neopeltolide also existed in the commercial fungicide pyribencarb and in the highly potent compound Crocacin derivative (Figure 1). Therefore, the crystal structure (PDB code: 3CWB)[27] of the chicken bc_1 complex bound to the Crocacin derivative was selected herein as the receptor model.

As is known, the bc_1 complex has two binding sites, the Q_o-site (a quinol oxidation site) and

the Q_i-site (a quinone reduction site). Then, neopeltolide was docked into the Q_o-site and the Q_i-site, producing two neopeltolide-bound complexes (Figure S1), referred to as the neopeltolide-Q_o complex and neopeltolide-Q_i complex, respectively. The binding energy obtained from AutoDock was -9.44 kcal/mol for the neopeltolide-Q_o complex and -8.90 kcal/mol for the neopeltolide-Q_i complex, indicating that the neopeltolide-Q_o complex was more favorable than the neopeltolide-Q_i complex. To further confirm the binding mode of neopeltolide, we performed 30 ns molecular dynamics simulations for the neopeltolide-Q_o and neopeltolide-Q_i complexes (Figure S2), and 200 snapshots obtained from the last 2 ns of each complex were used to calculate the binding energy using the MM/PBSA module. As shown in Table 1, the binding energies (ΔH) were -36.77 kcal/mol and -22.05 kcal/mol for the neopeltolide-Q_o and neopeltolide-Q_i complexes, respectively. The computational simulation results clearly showed that neopeltolide should bind to the Q_o-site of the bc_1 complex.

The comparison of the MD-simulated neopeltolide-Q_o complex with the known crystal structure of the Q_o-site inhibitor-bound bc_1 complex was very interesting. As shown in Figure 2, the complex structures of azoxystrobin (1SQB),[34] famoxadone (1L0L),[35] crocacin derivative (3CWB)[27] and stigmatellin (1PP9) [36] were superimposed. The common interaction with the bc_1 complex was that residues Glu271 and Phe274 (Figure 3A) separately formed H-bonds and a hydrophobic interaction with the inhibitor, indicating that the two residues played an important role in the binding of Q_o-site inhibitors. In addition, we observed that different types of inhibitors occupied relatively different spaces inside the Q_o pocket, although they shared some common binding area. For example, as shown in Figure 2, the phenoxypyrimidine moiety in azoxystrobin took on a nearly parallel conformation with the diphenyl-ether fragment in famoxadone, and their key pharmacophores (the methoxyacrylate fragment in azoxystrobin and oxazolidinedione fragment in famoxadone) formed the same H-bond with Glu271. The Crocacin derivative and stigmatellin showed some translation and then formed an additional new H-bond with His161, revealing an important binding site for the design of a Q_o-site inhibitor.

While considering the chemical structural similarity between neopeltolide and pyribencarb, we also compared the neopeltolide-Q_o complex with the binding model of pyribencarb[37-38] (Figure 3B) obtained from AutoDock. Similar to the classical Q_o-site inhibitor azoxystrobin, pyribencarb

also formed an H-bond with Glu271 and a hydrophobic interaction with Phe274. For neopeltolide-Q_o (Figure 3C, Figure S2B), its carbamate moiety inserted into the Q_o pocket and then formed an H-bond with Glu271. Meanwhile, the 14-membered macrolactone moiety of neopeltolide was located at the entrance of the Q_o-site and took on a relative extended conformation, forming hydrophobic interactions with residues Leu121, Met124, Phe128, Ile146, Phe150, Leu294, Leu299 and Phe274. The relative position of the neopeltolide in the Q_o-site was very similar to that of the crocacin derivative, but neopeltolide did not form an H-bond with His161.

Neopeltolide is attractive because its carbamate moiety gives it great potential to overcome the pathogen resistance associated with the G143A mutation.[7] Shimizu and his co-workers[37] reported that pyribencarb with a carbamate moiety as a pharmacophore showed a much lower resistance risk (R/S = 65 for *Botrytis cinerea* and 16 for *Sclerotinia sclerotiorum*) than kresoxim-methyl (R/S = 700 for *B. cinerea* and 580 for *S. sclerotiorum*) and azoxystrobin (R/S = 300 for *B. cinerea* and 1200 for *S. sclerotiorum*). Our computational simulations revealed that the steric clash between the inhibitors and residue Ala143 of the mutated bc_1 complex reduced the binding affinity of the inhibitors.[24] For the wide-type inhibitor-bound complex (Figure 3B), the distance between Gly143 and inhibitors ranged from 3.6 Å (*e.g.,* azoxystrobin) to 4.6 Å (*e.g.,* pyribencarb). The shorter the distance, the higher the resistance. Therefore, pyribencarb showed much lower resistance in the presence of the G143A mutation due to the greater distance between its carbamate moiety and the 143th residue. These results suggest that neopeltolide is a promising lead for the discovery of new bc_1 complex inhibitors to overcome the resistance associated with the G143A mutation.

Rational Design of Neopeltolide Analogs and Structural Optimization

The above computational simulations showed that His161 is an important binding site for Q_o-site inhibitors. However, neopeltolide did not form an H-bond with His161, possibly due to the lack of H-bond receptors of neopeltolide, which are marked by the black arrow in Figure 3C. Therefore, target molecules were designed by introducing an amide bond to replace the carboxylic ester moiety. Meanwhile, to simplify the chemical structure of neopeltolide, the butylene unit

between the carboxylic ester moiety and oxazole ring was deleted and the 14-membered macrolactone moiety of neopeltolide was replaced with a diphenyl-ether fragment. Our previous study[26] showed that the diphenyl-ether was a fragment that forms hydrophobic interactions with the protein. We have successfully designed a series of diphenyl-ether derivatives, especially those bearing the 2-Cl-4-CF_3 and 2-Cl-4-Cl group, as bc_1 complex inhibitors and complex II inhibitors (Figure 1). In addition, some other groups also reported a series of diphenyl-ether derivatives as bc_1 complex inhibitors.[39-40] Therefore, compounds **15~23** were first synthesized, and their activity against porcine SCR were tested and are shown in Table 2. The commercial fungicide azoxystrobin was selected as a positive control. Fortunately, compounds **21** (R^1 = H; R^2 = 2-Cl-4-CF_3) and **23** (R^1 = 3-Cl-5-Cl; R^2 = 2-Cl-4-Cl) showed good potency against porcine SCR, with IC_{50} values of 0.17 μM and 0.92 μM, respectively. These results indicated that our design strategy was reasonable and feasible.

Then, structural optimization was carried out with compound **21** as a new starting scaffold. To make the structure optimization more efficient, we first studied the binding mode of compound **21**. As shown in Figure 3D, compound **21** could form an H-bond with Glu271 and could interact hydrophobically with Phe274. However, unfortunately, compound **21** did not form an H-bond with His161. Superimposing its binding mode with that of pyribencarb, we found that the relative position of the carbamate pharmacophore of compound **21** was less deep than that of pyribencarb (Figure 3D) and the Crocacin derivative (Figure S3A). In other words, the carbamate pharmacophore of compound **21** did not match well with that of the pyribencarb and the Crocacin derivative. Keeping these differences in mind, we then focused on adjusting the relative position of the carbamate pharmacophore by inserting a CH_2 unit between the NH of the amide and phenyl ring of the diphenyl-ether or between the oxygen atom and the terminal phenyl ring of the diphenyl-ether to produce compounds **24~31** and **32~43**, respectively. The bioassay indicated that compounds **24~31** did not show improved potency, whereas six compounds from the second series displayed significantly improved inhibition activity against porcine SCR compared to compound **21** (IC_{50} = 0.17 μM). For example, the IC_{50} values of compounds **36**, **37**, **38**, **41**, **42**, and **43** were 0.047 μM, 0.039 μM, 0.082 μM, 0.067 μM, 0.044 μM and 0.021 μM, respectively, and had approximately 2- to 8-times higher potency that compound **21**.

Then, compound **43**, which had the highest potency, was selected as a representative compound to analyze its binding mode. As shown in Figure 3E, except for the H-bond interaction with Glu271, compound **43** formed an additional H-bond with His161. In addition, its diphenyl-ester moiety extended toward the entrance of the Q_o-site to form hydrophobic interactions with Phe274 and Phe128. As a consequence, the carbamate pharmacophore of compound **43** matched very well with that of the pyribencarb and Crocacin derivative (Figure S3B). The significantly increased potency of compound **43** confirmed that His161 is an important binding site, which should be taken into account when designing new bc_1 complex inhibitors. Because the diphenyl-ester formed a hydrophobic interaction with its surrounding residues, introducing a hydrophobic group onto the diphenyl-ester moiety is favorable for the binding affinity. For example, compounds **36** (3-Cl, IC_{50} = 0.047 μM), **37** (2-Br, IC_{50} = 0.039 μM) and **38** (3-Br, IC_{50} = 0.082 μM) showed higher activity than compound **33** (3-F, IC_{50} = 0.32 μM).

According to our previous study[25], improving the π-π stacking interaction with Phe274 will benefit the binding affinity. Then, a naphthalene ring was introduced to replace the terminal phenyl of diphenyl-ester moiety. Meanwhile, the amide bond was also replaced by an ester bond based on the isostere rule. As expected, the resulting compound, **44**, showed high inhibition activity against the porcine SCR, with an IC_{50} value of 0.047 μM. Similarly, introducing a bromo group into the naphthalene ring further improved the potency and produced compounds **45** and **46**, which had IC_{50} values of 0.012 μM and 0.016 μM, respectively. The binding mode of compound **45** to the bc_1 complex is shown in Figure 3F. Compound **45** formed a H-bond not only with Glu271 but also with His161. In addition, the naphthalene ring of **45** took on a more favorable π-π interaction with Phe274. The energy calculation results showed that compound **45** had the highest Van der Waals (VDW) energy (-77.06 kcal/mol) and the highest binding energy (ΔG_{cal} = -48.67 kcal/mol) of all the compounds. Notably, compared with neopeltolide, compound **45** had a slightly lower activity, but its chemical structure is much simpler and its synthesis is much easier. Therefore, compound **45** could be regarded as a new lead for the further discovery of bc_1 complex inhibitors.

Synthetic Chemistry

The titled compounds were synthesized by multiple-step routes, as shown in Scheme 1. In this synthetic procedure, (Z)-2-(3-((methoxycarbonyl)amino)prop-1-en-1-yl)oxazole-4- carboxylic acid **6** is a key intermediate for the titled compounds. Here, the cheap and commercially available 2-propynylamine (**1a**) and methyl chloroformate (**1b**) were selected as starting materials. The preparation of 4-((methoxycarbonyl)amino)but-2-ynoic acid **2** was achieved by carboxylation of prop-2-yn-1-ylcarbamate **1** with butyllithium in THF under a CO_2 atmosphere. Reduction of **2** with Lindlar's catalyst afforded (Z)-4-((methoxycarbonyl)- amino)but-2-enoic acid **3,** which reacted with L-serine methyl ester hydrochloride, N-methylmorpholine and isobutyl chloroformate to afford methyl(Z)-(4-((methoxycarbonyl)- amino)but-2-enoyl)serinate **4**. The intermediate **6** could be obtained by cyclization of **4** with DAST, DBU and $BrCCl_3$ at low temperature, followed by hydrolysis with lithium hydroxide to provide an excellent yield.

The substituted 4-diphenyl ether derivatives **8a-i, 10a-f, 12a-l** and **14a-c** moiety could be prepared in two routes (A, B) via a nucleophilic substitution reaction. In route A, substituted fluorobenzenes/phenols were reacted with the corresponding phenols/benzyl bromide to afford intermediates **7a-i** and **9a-f**, which were reduced with iron or zinc powder to afford intermediates **8a-i,** and **10a-f**. In route B, 4-fluorobenzaldehydes were reacted with substituted phenols or naphthols to afford **11a-l** and **13a-c**, which were reduced, respectively, with zinc powder or $NaBH_4$ to afford the key intermediates **12a-l** and **14a-c**. In the final step, condensation of 4-diphenyl ether derivatives **8a-i, 10a-f, 12a-l** and **14a-c** with intermediate **6** was performed to afford the corresponding target compounds **15~46.**

Computational Simulations

To understand the structure-activity relationship at the atomic level, we performed the molecular docking and binding free energy calculations for all the newly synthesized compounds according to previous methods.[41-43] The different kinds of binding energy (ΔG_{cal}, the calculated binding free energy; ΔE_{VDW}, the VDW energy; ΔE_{ele}, the electrostatic energy; ΔE_{np}, the nonpolar solvation energy; and ΔE_{polar}, the polar solvation energy) are shown in Table 4. The highest binding free energy (ΔG_{cal}) was -48.67 kcal/mol for compound **45**, and the lowest binding energy (ΔG_{cal}) was -40.31 kcal/mol for compound **32**. The corresponding experimental binding free

306 energy (ΔG_{exp}) was -10.84 kcal/mol for compound **45** and -8.47 kcal/mol for compound **32.**
307 Moreover, the ΔG_{exp} showed a qualitatively identical trend with ΔG_{cal}, and their correlation
308 coefficient of R^2 was 0.90 (Figure S4), further confirming the reliability of the computational
309 models constructed in the present study. In addition, the excellent correlation between ΔG_{cal} and
310 ΔG_{exp} also further proved that neopeltolide should belong to the Q_o-site inhibitor of the bc_1
311 complex.
312
313
314 In summary, the natural product neopeltolide was successfully assigned to be a Q_o site
315 inhibitor by integrating molecular docking, molecular dynamics simulations and MM/PBSA
316 calculations. Then, a series of neopeltolide derivatives, for use as new potent inhibitors of the bc_1
317 complex, were designed and synthesized, with neopeltolide as the template. Compound **45**,
318 (*Z*)-4-((7-bromonaphthalen-2-yl)-oxy)benzyl-2-(3-((methoxycarbonyl)amino)prop-1-en-1-yl)-
319 oxazole-4-carboxylate was identified as the most potent candidate, with an IC_{50} value of 12 nM
320 against porcine SCR. Further computational simulations revealed that most of the compounds
321 inside the Q_o-site of bc_1 complex formed a H-bond with Glu271 and a π-π interaction with Phe274,
322 while the most active compound (compound **45**) formed an additional H-bond with His161. These
323 results indicate that Glu271, Phe274 and His161 are the key residues for designing bc_1 complex
324 inhibitors.
325
326 **Supplementary Data**
327 Supplementary data associated with this article can be found in the online version, at
328 http://pubs.acs.org/.
329
330 **AUTHOR INFORMATION**
331 Corresponding Author *E-mail: (GFY) gfyang@mail.ccnu.edu.cn
332
333 **Funding**
334 The research was supported in part by the National Key Research and Development Program of

China (2017YFD0200506), the National Natural Science Foundation of China (No. 21837001, 21472065, 21772057), and the Program of Introducing Talents of Discipline to Universities of China (111 program, B17019).

Notes

The authors declare no competing financial interest.

References:

1. Chen, C.; Wu, Q. Y.; Shan, L. Y.; Zhang, B.; Verpoort, F.; Yang, G. F. Discovery of cytochrome bc1 complex inhibitors inspired by the natural product karrikinolide. *RSC. Adv*. **2016**, *6*, 97580-97586.
2. Xia, D.; Esser, L.; Yu, L.; Yu, C. A. Structural basis for the mechanism of electron bifurcation at the quinol oxidation site of the cytochrome bc1 complex. *Photosynth Res.* **2007**, *92*, 17-34.
3. Crofts, A. R. The Cytochrome bc1 complex: Function in the Context of Structure. *Annu. Rev. Physiol*. **2004**, *66*, 689-733.
4. Kim, H.; Xia, D.; Yu, CA.; Xia, JZ.; Kachurin, AM.; Zhang, L.; Yu, L.; Deisenhofer, J. Inhibitor binding changes domain mobility in the iron-sulfur protein of the mitichondrial bc1 complex from bovine heart. *Proc. Natl. Acad. Sci. USA.* **1998**, *95*, 8026-8033.
5. Berry, E. A.; Guergova-Kuras, M.; Huang, L. S.; Crofts, A. R. Structure and Function of Cytochrome bc1 Complexes. *Annu. Rev. Biochem*. **2000**, *69*, 1005-1075.
6. Lee, J. W.; Chan, M.; Law, T. V.; Kwon, H. J.; Jap, B. K. Preliminary cryocrystallographic study of the mitochondrial cytochrome bc1 complex: improved crystallization and flash-cooling of a large membrane protein. *J. Mol. Biol.* **1995**, *252*, 15-19.
7. Bartlett, D. W.; Clough, J. M.; Godwin, J. R.; Hall, A. A.; Hamer, M.; Parr-Dobrzanski, B. The strobilurin fungicides. *Pest Manag. Sci.* **2002**, *58*, 649-662.
8. Dufour, M. C.; Fontaine, S.; Montarry, J.; Corio-Costeta, M. F. Assessment of fungicide resistance and pathogen diversity in Erysiphe necator using quantitative real-time PCR assays. *Pest Manag. Sci*. **2011**, *67*, 60-69.

9. Fisher, N.; Meunier, B. Molecular basis of resistance to cytochrome bc_1 inhibitors. *FEMS Yeast Res.* **2008**, *8*, 183-192.
10. Fuwa, H.; Noto, K.; Kawakami, M.; Sasaki, M. Synthesis and Biological Evaluation of Aspergillide A/Neopeltolide Chimeras. *Chem. Lett*. **2013**, *42*, 1020-1022.
11. Lin, L.; Mulholland, N.; Wu, Q. Y.; Beattie, D.; Huang, S. W.; Irwin, D.; Clough, J.; Gu, Y. C.; Yang, G. F. Synthesis and Fungicidal Activity of Novel Sclerotiorin Analogues. *J. Agric. Food Chem.* **2012**, *60*, 4480-4491.
12. Wright, A. E.; Botelho, J. C.; Guzmán, E.; Harmody, D.; Linley, P.; McCarthy, P. J.; Pitts, T. P.; Pomponi, S. A.; Reed, J. K. Neopeltolide, a Macrolide from a Lithistid Sponge of the Family Neopeltidae. *J. Nat. Prod*. **2007**, *70*, 412-416.
13. Ulanovskaya, O. A.; Janjic, J.; Suzuki, M.; Sabharwal, S. S.; Schumacker, P. T.; Kron, S. J.; Kozmin, S. A. Synthesis enables identification of the cellular target of leucascandrolide A and neopeltolide. *Nat. Chem. Biol.* **2008**, *4*, 418-424.
14. Vintonyak, V. V.; Kunze, B.; Sasse, F.; Maier, M. E. Total Synthesis and Biological Activity of Neopeltolide and Analogues. *Chem. Eur. J*. **2008**, *14*, 11132-11140.
15. Custar, D. W.; Zabawa, T. P.; Hines, J.; Crews, C. M.; Scheidt, K. A. Total Synthesis and Structure-Activity Investigation of the Marine Natural Product Neopeltolide. *J. Am. Chem. Soc*. **2009**, *131*, 12406-12414.
16. Cui, Y.; Balachandran, R.; Day, B. W.; Floreancig, P. E. Synthesis and Biological Evaluation of Neopeltolide and Analogs. *J. Org. Chem*. **2012**, *77*, 2225-2235.
17. Fuwa, H.; Kawakami, M.; Noto, K.; Muto, T.; Suga, Y.; Konoki, K.; Sasaki, M. Concise Synthesis and Biological Assessment of (+)-Neopeltolide and a 16-Member Stereoisomer Library of 8,9-Dehydroneopeltolide: Identification of Pharmacophoric Elements. *Chem. Eur. J*. **2013**, *19*, 8100-8110.
18. Fuwa, H.; Noguchi, T.; Kawakami, M.; Sasaki, M. Synthesis and biological evaluation of (+)-neopeltolide analogues: Importance of the oxazole-containing side chain. *Bioorg. Med. Chem. Lett*. **2014**, *24*, 2415-2419.
19. Fuwa, H.; Saito, A.; Naito, S.; Konoki, K.; Sasaki, M. Total Synthesis and Biological Evaluation of (+)-Neopeltolide and Its Analogues. *Chem. Eur. J*. **2009**, *15*, 12807-12818.

393 20. Wang, M. Y.; Wang, F.; Hao, G. F.; Yang, G. F. FungiPAD: A free web tool for compound
394 property evaluation and fungicide-like analysis. *J. Agric. Food Chem.* **2019**, *67*, 1823-1830.
395 21. Fisher, N.; Bourges, I.; Hill, P.; Brasseur, G.; Meunier, B. Disruption of the interaction
396 between the Rieske iron-sulfur protein and cytochrome b in the yeast bc1 complex owing to a
397 human diseaseassociated mutation within cytochrome *b*. *Eur. J. Biochem*. **2004,** *271*,
398 1292-1298.
399 22. Wang, TSY.; Tsou, C.L.; Wang, Y.L. Studies On Succinic Dehydrogenase II. Further
400 Observations on the Properties of the Enzyme and its Prosthetic Group. *Scientia Sinica*, **1958**,
401 *7*, 65-75.
402 23. Zhu, X. L.; Xiong, L.; Li, H.; Song, X. Y.; Liu, J. J.; Yang, G. F. Computational and
403 Experimental Insight into the Molecular Mechanism of Carboxamide Inhibitors of
404 Succinate-Ubquinone Oxidoreductase. *ChemMedChem*. **2014***, 9,* 1512-1521.
405 24. Zhu, X. L.; Zhang, M. M.; Liu, J. J.; Ge, J. M.; Yang, G. F. Ametoctradin is a Potent Qo Site
406 Inhibitor of the Mitochondrial Respiration Complex III. *J. Agric. Food. Chem*. **2015**, *63*,
407 3377-3386.
408 25. Zhao, P. L.; Wang, L.; Zhu, X. L.; Huang, X.; Zhan, C. G.; Wu, J. W.; Yang, G. F.
409 Subnanomolar inhibitor of cytochrome bc1 complex designed by optimizing interaction with
410 conformationally flexible residues. *J. Am. Chem. Soc*. **2010**, *132*, 185-194.
411 26. Xiong, L.; Li, H.; Jiang, L. N.; Ge, J. M.; Yang, W. C.; Zhu, X. L.; Yang, G. F.
412 Structure-Based Discovery of Potential Fungicides as Succinate Ubiquinone Oxidoreductase
413 Inhibitors. *J. Agric. Food Chem*. **2017**, *65*, 1021-1029.
414 27. Crowley, P. J.; Berry, E. A.; Cromartie, T.; Daldal, F.; Lee, D. W.; Phillips, J. E.; Taylor, A.;
415 Viner, R. The role of molecular modeling in the design of analogues of the fungicidal natural
416 products crocacins A and D. *Bioorg. Med. Chem.* **2008**, *16*, 10345-10355.
417 28. Morris, G. M.; Goodsell, D. S.; Halliday, R. S.; Huey, R.; Hart, W. E.; Belew, R. K.; Olson,
418 A. J. Automated docking using a Lamarckian genetic algorithm and an empirical binding free
419 energy function. *J. Comput. Chem.* **1998**, *19*, 1639-1662.
420 29. Case, D. A.; Cheatham, T. E., III.; Darden, T.; Gohlke, H.; Luo, R.; Merz, K. M., Jr.;
421 Onufriev, A.; Simmerling, C.; Wang, B.; Woods, R. The Amber biomolecular simulation

422 programs. *J. Comput. Chem*. **2005**, *26*, 1668-1688.
423 30. Ponder, J. W.; Case, D. A. Force fields for protein simulations. *Adv. Protein Chem*. **2003**, *66*,
424 27-85.
425 31. Sitkoff, D.; Sharp, K. A.; Honig, B. Accurate calculation of hydration free energies using
426 macroscopic solvent models. *J. Phys. Chem*. **1994**, *98*, 1978-1988.
427 32. Connolly, M. L. Analytical molecular surface calculation. *J. Appl. Crystallogr*. **1983**, *16*,
428 548-558.
429 33. Fehr, M.; Wolf, A.; Stammler, G. Binding of the respiratory chain inhibitor Ametoctradin to
430 mitochondrial bc1 complex. Pest Manag. Sci. **2015,** 72, 591-602.
431 34. Esser, L.; Quinn, B.; Li, Y. F.; Zhang, M.; Elberry, M.; Yu, L.; Yu, C.A.; Xia, D.
432 Crystallographic studies of quinol oxidation site inhibitors: a modified classification of
433 inhibitors for the cytochrome bc(1) complex. *J. Mol. Biol*. **2004**, *341*, 281-302.
434 35. Wu, N.; Pai, E. F. Crystal structures of inhibitor complexes reveal an alternate binding mode
435 in orotidine-5'-monophosphate decarboxylase. *J. Biol. Chem*. **2002**, *277*, 28080-28087.
436 36. Huang, L. S.; Cobessi, D.; Tung, E.Y.; Berry, E. A. Binding of the Respiratory Chain
437 Inhibitor Antimycin to the Mitochondrial bc(1) Complex: A New Crystal Structure Reveals
438 an Altered Intramolecular Hydrogen-bonding Pattern. *J. Mol. Biol*. **2005**, *351*, 573-597.
439 37. Kataoka, S.; Takagaki, M.; Kaku, K.; Shimizu, T. Mechanism of action and selectivity of a
440 novel fungicide, pyribencarb. *J. Pestic. Sci*. **2010**, *35*, 99-106.
441 38. Takagaki, M.; Ozaki, M.; Fujimoto, S.; Fukumoto, S. Development of a novel fungicide,
442 pyribencarb. *J. Pestic. Sci.* **2014**, *39*, 177-178.
443 39. Bueno, J. M.; Herreros, E.; Angulo-Barturen, I.; Ferrer, S.; Fiandor, J. M.; Gamo, F. J.;
444 Gargallo-Viola, D.; Derimanov, G. Exploration of 4(1H)-pyridones as a novel family of
445 potent antimalarial inhibitors of the plasmodial cytochrome bc1. *Future Med. Chem*. **2012,** *4*,
446 2311-2323.
447 40. Yeates, C. L.; Batchelor, J. F.; Capon, E. C.; Cheesman, N. J.; Fry, M.; Hudson, A. T.;
448 Pudney, M.; Trimming, H.; Woolven, J.; Bueno, J. M.; Chicharro, J.; Fernández, E.; Fiandor,
449 J. M.; Gargallo-Viola, D.; Gómez de las Heras F.; Herreros, E.; León, M. L. Synthesis and
450 structure-activity relationships of 4-pyridones as potential antimalarials. *J Med Chem*. **2008,**

51, 2845-2852.

41. Yan, F. F.; Liu, X.G.; Zhang, S.L.; Su, J.; Zhang, Q.G.; Chen, J.Z. Molecular Dynamics Exploration of Selectivity of Dual Inhibitors 5M7, 65X, and 65Z toward Fatty Acid Binding Proteins 4 and 5. *Int. J. Mol. Sci*. **2018**, *19*, 2496-2514.
42. Chem, J.Z.; Wang, J.N.; Zhu, W.L. Zinc ion-induced conformational changes in new Delphi metallo-β-lactamase 1 probed by molecular dynamics simulations and umbrella sampling. *Phys. Chem. Chem. Phys.*, **2017**, *19*, 3067-3075.
43. Chem, J.Z.; Wang, X.Y.; Zhu, T.; Zhang, Q.G.; Zhang, Z.H.John. A Comparative Insight into Amprenavir Resistance of Mutations V32I, G48V, I50V, I54V, and I84V in HIV-1 Protease Based on Thermodynamic Integration and MM-PBSA Methods. *J. Chem. Inf. Model.,* **2015**, *55*, 1903−1913

44. FIGURE CAPTIONS

Scheme 1. Synthetic route for the target compounds **15~46**.

Figure 1. Design protocol of the target compound.

Figure 2. Relative position of known bc_1 complex inhibitors in the Q_o-site. The PDB structures (1SQB, 1L0L, 1PP9, and 3CWB) were used. Among them, famoxadone and azoxystribin were commercial fungicides, and stigmatellin and crocacin-derivative were high potency inhibitors. For clarity, the long hydrophobic chain of stigmatellin was not displayed.

Figure 3. (A) Binding mode of the Crocacin derivative (yellow stick) with the bc_1 complex (PDB ID 3CWB). (B) The binding mode overlay of pyribencarb (brown stick) with Azoxystrobin (ice blue stick, 1SQB). The closest distance between the ligand with G143 was measured. (C) The binding mode of neopeltolide (yellow stick) with the bc_1 complex. (D) The binding mode of compound **21** (yellow stick) overlaid with pyribencarb (brown stick). (E) The binding mode of compound **43** (yellow stick) overlaid with pyribencarb (brown stick). (F) The binding mode of compound **45** (yellow stick) overlaid with pyribencarb (brown stick).

Figure 4. Kinetic analysis of inhibition by azoxystrobin (A) and compound **45** (B) against porcine SCR. (A) Azoxystrobin is noncompetitive with respect to cytochrome *c*. The reaction mixture contains 100 mM PBS (pH 7.4), EDTA (0.3 mM), succinate (20 mM), cytochrome *c* (3-60 μM), an appropriate amount of SCR, and a series of concentrations of azoxystrobin (0 nM; 70 nM; 200 nM; 500 nM). (B) Compound **45** is noncompetitive with respect to cytochrome *c*. The reaction mixture contains 100 mM PBS (pH 7.4), EDTA (0.3 mM), succinate (20 mM), cytochrome *c* (3-60 μM), an appropriate amount of SCR, and a series of concentrations of **45** (0 nM; 100 nM; 200 nM; 300 nM).

Table 1. Binding energy of neopeltolide in the Q_o and Q_i sites (kcal/mol)

Table 2. Percent inhibition and IC_{50} value of the title compounds against porcine SCR.

Table 3. IC_{50} value of the title compounds against porcine SCR.

Table 4. Individual energy terms of the calculated binding energies of the title compounds (kcal/mol)

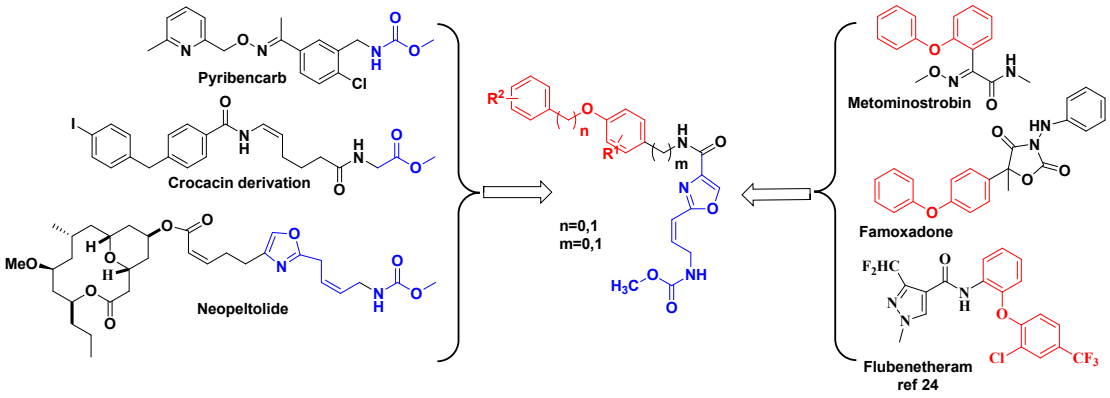

Figure 1. Design protocol of the target compounds

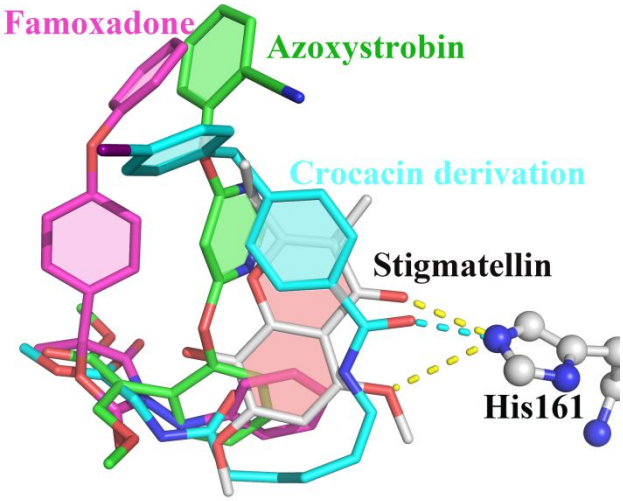

Figure 2. Relative position of known bc1 complex inhibitors in the Qo-site. The PDB structures (1SQB, 1L0L, 1PP9, and 3CWB) were used. Among them, famoxadone and azoxystribin were commercial fungicides, and stigmatellin and crocacin-derivative were high potency inhibitors. For clarity, the long hydrophobic chain of stigmatellin was not displayed. .

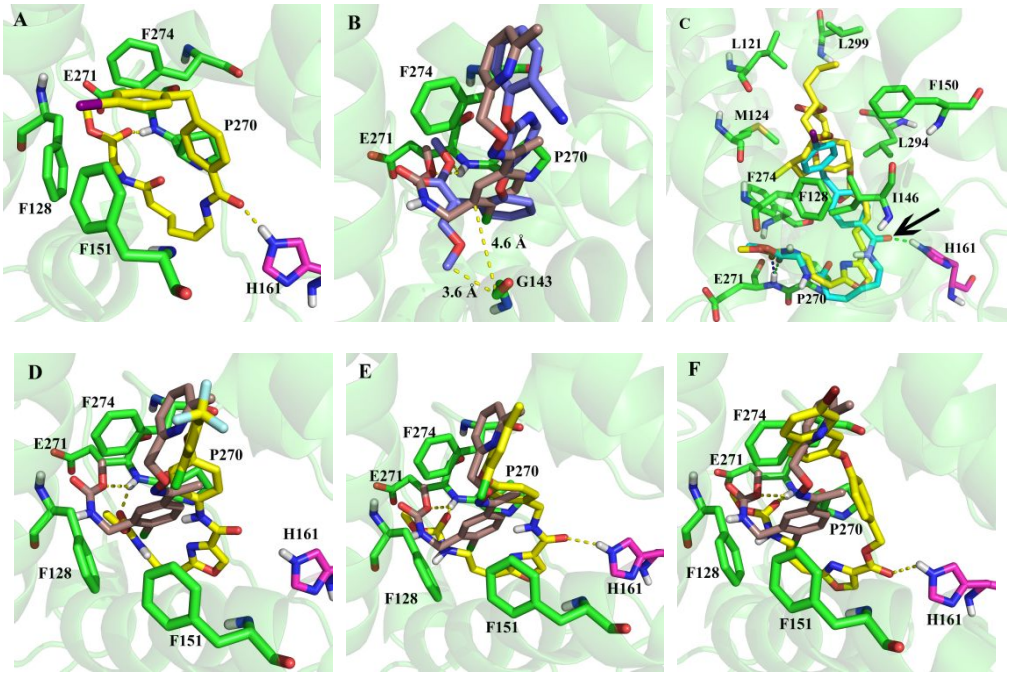

Figure 3. (A) Binding mode of the Crocacin derivative (yellow stick) with the bc1 complex (PDB ID 3CWB). (B) The binding mode overlay of pyribencarb (brown stick) with Azoxystrobin (ice blue stick, 1SQB). The closest distance between the ligand with G143 was measured. (C) The binding mode of neopeltolide (yellow stick) with the bc1 complex. (D) The binding mode of compound 21 (yellow stick) overlaid with pyribencarb (brown stick). (E) The binding mode of compound 43 (yellow stick) overlaid with pyribencarb (brown stick). (F) The binding mode of compound 45 (yellow stick) overlaid with pyribencarb (brown stick).

Scheme 1. Synthetic route for the target compounds **15-46**.

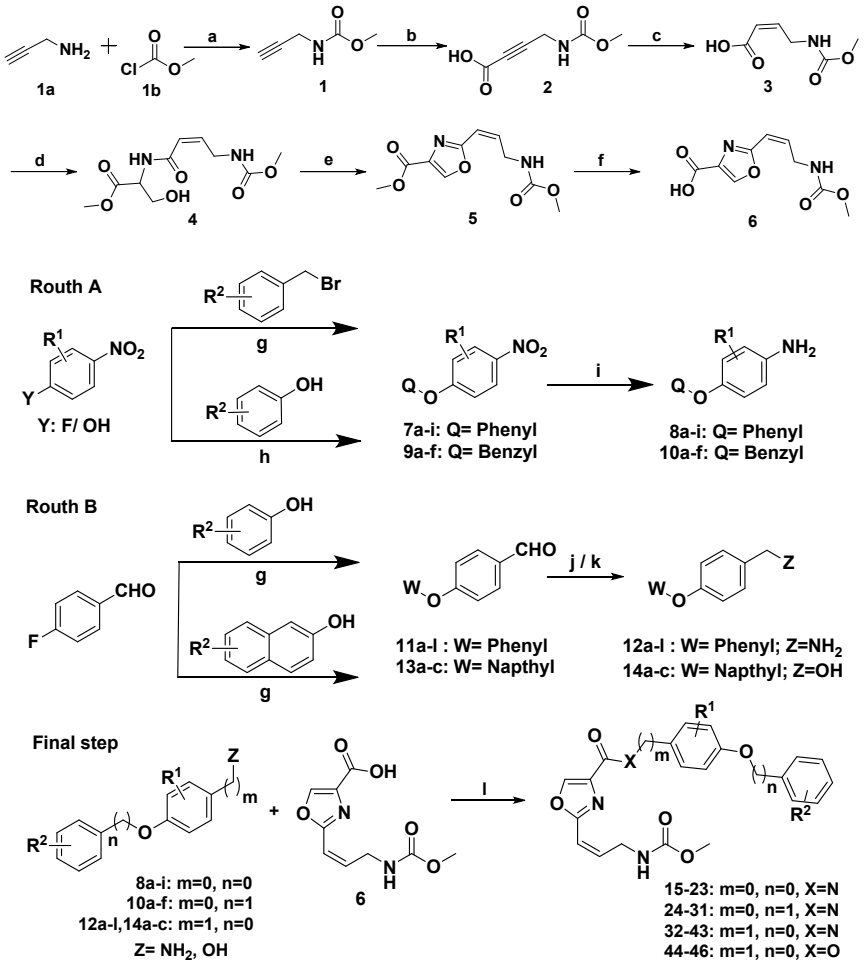

Reagents and conditions: (a) $NaHCO_3$,1,4-dioxane; (b) CO_2, n-BuLi, THF, -78°C; (c)H_2, Lindlar's catalyst, EtOAc; (d) L-serine methyl ester hydrochloride, i-BuOCOCl, N-Me-Morpholine, THF; (e) (1) DAST,CH_2Cl_2, -78°C (2) $BrCCl_3$, DBU, -20°C; (f) LiOH,THF/H_2O; (g) K_2CO_3, Acetone, reflux; (h) K_2CO_3, DMF, reflux; (i) Fe,NH_4Cl, EtOH/H_2O, reflux; (j) (1) $NH_2OH{\cdot}HCl$,$NaHCO_3$, EtOH, reflux; (2) Zn, HCl, EtOH/H_2O, reflux; (k) $NaBH_4$,THF/H_2O; (l) EDCI, HOBt, Et_3N, CH_3CN/THF. The yield of compound ranges from 8.7% to 91%, and detailed information is supported in the supporting information.

Table 1. Binding energy of neopeltolide in the Q_o and Q_i sites (kcal/mol)

	AutoDock binding Energy	ΔE_{VDW}[a]	ΔE_{Ele}[a]	ΔE_{polar}[a]	ΔE_{np}[a]	ΔH[a]
neopeltolide-Q_o	-9.44	-70.79	-10.51	50.93	-6.40	-36.77
neopeltolide-Q_i	-8.90	-50.23	-12.74	46.54	-5.62	-22.05

[a] Obtained from the 30 ns MD.

Table 2. Percent inhibition and IC_{50} (μM) value of the title compounds against porcine SCR

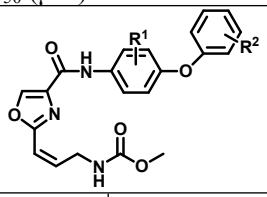

No.	R^1	R^2	IC_{50} or I%
15	3-Cl	2-Cl-4-CF_3	34%
16	3-Cl-5-Cl	2-Cl-4-CF_3	30%
17	3-Br	2-Cl-4-CF_3	49%
18	2-Me	2-Cl-4-CF_3	55%
19	3-Me	2-Cl-4-CF_3	42%
20	2-OMe	2-Cl-4-CF_3	59%
21	H	2-Cl-4-CF_3	0.17±0.016
22	3-Cl	2-Cl-4-Cl	14%
23	3-Cl-5-Cl	2-Cl-4-Cl	0.92±0.013
	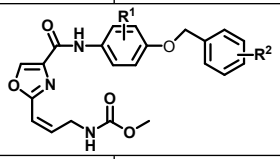		
24	H	4-Br	0.35±0.010
25	H	3-Br	3.71±0.19
26	H	H	11%
27	H	4-Me	16%
28	H	3-OMe	<10%
29	H	2-Cl-4-Cl	22%
30	H	3-F	<10%
31	H	3-F-5-F	<10%
	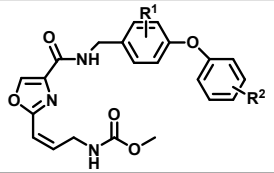		
32	H	2-F	0.64±0.01
33	H	3-F	0.32±0.01
34	H	4-F	0.33±0.01
35	H	2-Cl	0.15±0.01
36	H	3-Cl	0.047±0.02
37	H	2-Br	0.039±0.01
38	H	3-Br	0.082±0.01
39	H	3-Me	0.11±0.01
40	H	2-Cl-4-Cl	0.15±0.01
41	H	2-Cl-3-F	0.067±0.01
42	H	2-Cl-4-F	0.044±0.01
43	H	2-Cl-4-Me	0.021±0.01
azoxystrobin	-	-	0.205±0.010

Table 3. IC_{50} (μM) value of the title compounds against porcine SCR.

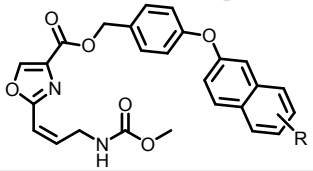

No.	R	IC_{50}	No.	R	IC_{50}
44	H	0.045±0.001	45	7-Br	0.012±0.002
46	6-Br	0.016±0.001	azoxystrobin	-	0.205±0.010

Table 4. Individual energy terms of the calculated binding energies of the titled compounds (kcal/mol)

Compound	ΔE_{VDW}	ΔE_{Ele}	ΔE_{Polar}	ΔE_{np}	ΔG_{cal}	ΔG_{exp}[a]
21	-68.11	-15.16	45.54	-4.92	-42.65	-9.26
32	-65.31	-32.51	62.47	-4.96	-40.31	-8.47
33	-63.66	-36.08	60.69	-4.89	-43.94	-8.88
34	-61.02	-29.50	54.20	-4.88	-41.20	-8.86
35	-67.28	-21.04	49.54	-5.00	-43.78	-9.33
36	-70.63	-21.86	50.21	-5.11	-47.40	-10.02
37	-65.58	-27.02	49.91	-5.15	-47.83	-10.13
38	-67.80	-31.85	58.75	-4.94	-45.84	-9.69
39	-68.53	-21.57	49.56	-5.16	-45.69	-9.52
40	-66.16	-23.34	50.45	-5.32	-44.37	-9.33
41	-67.01	-23.26	48.60	-5.18	-46.86	-9.81
42	-65.57	-26.66	49.99	-5.24	-47.49	-10.06
43	-66.94	-26.70	51.26	-5.35	-47.74	-10.50
44	-75.18	-21.74	55.23	-5.44	-47.14	-10.04
45	-77.06	-21.74	55.70	-5.58	-48.67	-10.84
46	-73.95	-21.08	51.82	-5.45	-48.66	-10.65

[a] $\Delta G_{exp} = -RTLnIC_{50}$

Graphical Abstract